Title
Nonlinear Structural Model Parameter Updating Using Residual Drift Measurements from Sequential Seismic Events

Journal
Journal of Structural Engineering, 151(12)

ISSN
0733-9445

Authors
De, Budhaditya
Burton, Henry V

Publication Date
2025-12-01

DOI
10.1061/jsendh.steng-15117

ASCE

Nonlinear Structural Model Parameter Updating Using Residual Drift Measurements from Sequential Seismic Events

Budhaditya De, S.M.ASCE[1]; and Henry V. Burton, Ph.D., S.E., M.ASCE[2]

Abstract: Model parameter updating can enhance the use of nonlinear structural response simulation to guide decision-making in the postearthquake environment. Since most structures in high seismic regions are not instrumented with sensors, the response history during ground shaking is usually not available after an earthquake. Nevertheless, technologies such as Light Detection and Ranging (LiDAR) and drone-mounted imaging devices have made it possible to more effectively measure residual deformations after the shaking has subsided. It is within this context that a framework for performing nonlinear structural model parameter updating based only on residual drift measurements is proposed. The considered setting is one where a structure is subjected to a sequence of ground motions (without repairs), whereby after each event, the structural model parameters are updated using a Bayesian formulation and the measured residual drift. The methodology is demonstrated by using experimental data from a reinforced concrete bridge pier subjected to six back-to-back ground motions with significant residual drifts recorded after the third, fourth, and fifth records in the sequence. The results showed that the updating procedure is able to incrementally (after each record) improve the accuracy of both the concrete and steel model parameters which also enhanced the estimates of the simulated peak and residual drifts. Finally, a sensitivity analysis is also carried out using an Extreme Gradient Boosting (XGBoost) machine learning model to assess the relative influence of the model parameters on the peak and residual drifts of the bridge pier. **DOI: 10.1061/JSENDH.STENG-15117.** *© 2025 American Society of Civil Engineers.*

Author keywords: Model parameter updating; Nonlinear structural analysis; Residual drift; Sequential earthquake events; Damage prediction; Sensitivity analysis.

Introduction

Understanding and quantifying the residual capacity of damaged structures is key to decision-making in the postearthquake environment. After a major seismic event, owners and operators of buildings and other infrastructure must decide if an affected facility is safe enough to resume occupancy. In some situations, the state of the affected infrastructure can be obviously determined from visual inspections. These cases usually involve structures that are clearly undamaged, or where the damage is so severe that the unsafe state is obvious. In other cases, the damage to the structure may be hidden or, despite being visible, the impact on the residual capacity cannot be determined only from visual inspections. For structures (e.g., buildings or bridges) that are instrumented with strong motion sensors (i.e., typically accelerometers), these measurement systems can inform the safety state of the structure.

The structural health monitoring (SHM) research literature contains numerous studies that utilize response measurements to assess the postearthquake safety state of structures (Naeim et al. 2005; Goulet et al. 2015; Reuland et al. 2019). Some of these methods rely on numerical modeling in combination with the response measurements to assess the safety state (Conde et al. 2017; De Domenico et al. 2022). Others utilize purely data-driven models where the response data is used to directly determine the level of structural (and sometimes nonstructural) damage (Zhang et al. 2018; Allali et al. 2018). For noninstrumented structures, nonlinear structural modeling can still be utilized to evaluate the residual structural capacity, especially if ground motions from the damaging event become available in the near term (i.e., in the days or weeks following the event).

As mentioned previously, nonlinear structural modeling and performance assessment is often used to guide decisions about the postearthquake residual capacity and safety state of damaged structures. This premise has been underscored not only in the research literature (Maeda et al. 2004; Mackie and Stojadinovic 2004) but also in guidelines that have been developed for use in practice (FEMA 2000). In both these domains, the importance of residual drifts as an indicator of the reduction in the lateral force–resisting system (LFRS) capacity of a damaged structure has been emphasized (FEMA 2018, 2020). This issue has been extensively studied in the research literature using nonlinear structural modeling and performance-based assessment. This usually involves a multistep process where a structural system is subjected to back-to-back or sequential ground motions.

The engineering demand parameters (EDPs) from the first ground motion can then be visually or statistically linked to the postearthquake residual capacity, as measured by the response or damaged state under subsequent records. The EDPs recorded under the initial event often include the peak transient and residual drifts with more local (i.e., component-level) response demands being sometimes used. Several studies have shown that compared with peak transient demands, residual deformations (local or global) also have

[1]Doctoral Candidate, Dept. of Civil and Environmental Engineering, Univ. of California, Los Angeles, CA 90085 (corresponding author). ORCID: https://orcid.org/0009-0009-5599-5619. Email: budhaditya@g.ucla.edu

[2]Associate Professor, Dept. of Civil and Environmental Engineering, Univ. of California, Los Angeles, CA 90085.

Note. This manuscript was submitted on March 3, 2025; approved on July 15, 2025; published online on October 11, 2025. Discussion period open until March 11, 2026; separate discussions must be submitted for individual papers. This paper is part of the ***Journal of Structural Engineering***, © ASCE, ISSN 0733-9445.

considerable correlation with postearthquake structural performance (McCormick et al. 2008; Ruiz-García and Miranda 2006; Pampanin et al. 2003; Mackie and Stojadinovic 2004). These findings highlight the critical need to accurately simulate residual deformations in nonlinear structural models that are used in postearthquake structural safety assessments.

Model parameter updating is a well-known strategy for reducing the uncertainty in EDP estimates generated using structural response simulation. Prior studies in this area can be categorized based on several factors. For instance, the type of structure considered has ranged from highly idealized single-degree-of-freedom (SDOF) systems (Hemez and Doebling 2001) to more realistic multi-degree-of-freedom (MDOF) structures (Wu and Li 2004). The type of response demand used as the basis of the model parameter updating or objective function has also differed among prior studies, with some investigators using peak responses (e.g., peak story drift or peak component deformation) (Yu et al. 2022b), whereas others utilized cumulative or history-based responses (e.g., the entire response history or cumulative energy) (Ebrahimian et al. 2017). Several different types of algorithms have also been used to produce the updated parameter values. Strategies rooted in Bayesian statistics are commonplace in these types of studies (Astroza et al. 2017). Others have relied on advanced optimization routines (Ren and Chen 2010) and machine learning approaches (Zhang and Sun 2021; Marwala 2010).

The source of the observed or measured data is a major consideration for the practical or real-world application of these model updating strategies. Some prior investigations use responses from laboratory experiments (Friswell et al. 2001) or simulations (Ebrahimian et al. 2015) to demonstrate newly developed updating methods, whereas others employed data from real instrumented buildings (Jaishi and Ren 2005). Of these three sources, the latter is the only one that is feasible for real-world applications. However, most structures are not instrumented with accelerometers so the complete response history during ground shaking will not be available.

This raises the issue of whether there are measurements that can be taken after the shaking has ended that can be used as the observed responses. A couple of studies have tried to address this issue by using measured residual drifts to update estimates of peak transient story drifts (Yazgan and Dazio 2012; Dai et al. 2017). However, these studies were not focused on model parameter updating, which significantly limits their applicability to comprehensive performance-based assessments under sequential earthquake loading.

This paper presents a framework for performing nonlinear structural model parameter updating in the postearthquake environment, where there is the possibility of sequential events that occur after the mainshock. To broaden the practical applicability of the proposed methodology, only residual drifts that are observable/measurable postshaking are used as the observed responses and the basis for the model updating procedure. It is worth noting that various new technologies such as camera-mounted drones (Yu et al. 2022a) and Light Detection and Ranging (LiDAR) (Foroughnia et al. 2024) have been validated as sources of residual deformation measurements in earthquake-damaged structures.

The proposed framework utilizes a sequential updating strategy, whereby expected values of the structural model parameters are initially used to replicate the response demands from the first event. Then, using the residual drift measurements from that same event, an updating methodology is implemented to obtain the posterior estimates of the model parameters. The updated model can then be used to estimate the response demands for subsequent events in the postmainshock environment. In other words, for a given earthquake sequence, the response demands from the ith event can be estimated using a model that is updated using the residual drifts from the $i-1$th event. The sequential updating generates increasingly better estimates of the parameters (i.e., closer to their true values) following each event in the sequence. This in turn produces more realistic EDP predictions and structural damage assessments, thereby enhancing decision-making in the aftershock environment.

The procedure is demonstrated using the results of a physical experiment conducted at the University of California, San Diego (UCSD), outdoor shake table, where a bridge pier was subjected to six sequential ground motions that produced nontrivial residual drift demands (starting from the third record in the sequence) (Schoettler et al. 2012). The choice of the experiment was guided by its uniqueness both in terms of the number of applied back-to-back ground motions and the meaningful residual drift demands that were produced. A sensitivity analysis was also performed to determine which model parameters should be prioritized during the updating process.

The next section provides a brief overview of the framework, which is followed by the theoretical formulation of the parameter estimation procedure. The application of the sequential model parameter updating approach to the bridge pier experiment is then described in detail. Subsequently, the results of the sensitive analysis are presented, followed by a summary of the key findings, limitations, and suggestions for future related work.

Framework Overview

A schematic overview of the methodology used to update nonlinear structural model parameters under sequential seismic events is presented in Fig. 1. Prior to the initial event (E_1), it was assumed that there is an existing nonlinear model that has been established as part of the postearthquake structural safety assessment decision-making protocol. Initially constructed using the best estimate expected value of the parameters ($\mathbb{E}[\mathbf{\Theta}_0]$), this model can be used to estimate the structural response under the first event prior to performing any residual drift measurements. In fact, by simulating the response of the structure under E_1 based on $\mathbb{E}[\mathbf{\Theta}_0]$, this model can inform the decision regarding whether a detailed in-person inspection is needed.

If a ground motion recording at or near the site of interest is available, it can be used for this initial response estimation. Otherwise, a suite of ground motions scaled to the expected target spectra (determined using ground motion models and information about the event) can be used for this initial analysis. In this situation (i.e., recorded ground motion unavailable), the record-to-record uncertainty would need to be propagated into the response history analysis. Model parameter estimation can also be propagated by infusing Monte Carlo simulation into the response history analysis. This would require having complete probability distributions of the model parameters, $f_{\Theta_0}(\Theta_0)$ instead of only the expected values. The details of this Monte Carlo–based response history analysis are discussed later in the paper.

If the damage under E_1 is substantial, the residual drift in the structure is measured and recorded as $\mathrm{RDR}_{\mathrm{obs},1}$. Using the parameter estimation formulation detailed subsequently in the paper, the nonlinear structural model parameters can be updated ($f_{\Theta_1}(\Theta_1) = f_{\Theta_0}(\Theta_0|\mathrm{RDR}_{\mathrm{obs},1})$) and used to repeat the response history analysis under E_1. This would produce an updated set of the EDPs that, ideally, would be closer to the true distribution compared with the initial analysis. The initial set of model parameters, $f_{\Theta_0}(\Theta_0)$, would serve as inputs into the model parameter updating procedure. When the next major event in the sequence (E_2) occurs, the model parameters updated based on $\mathrm{RDR}_{\mathrm{obs},1}$ can be initially used for the

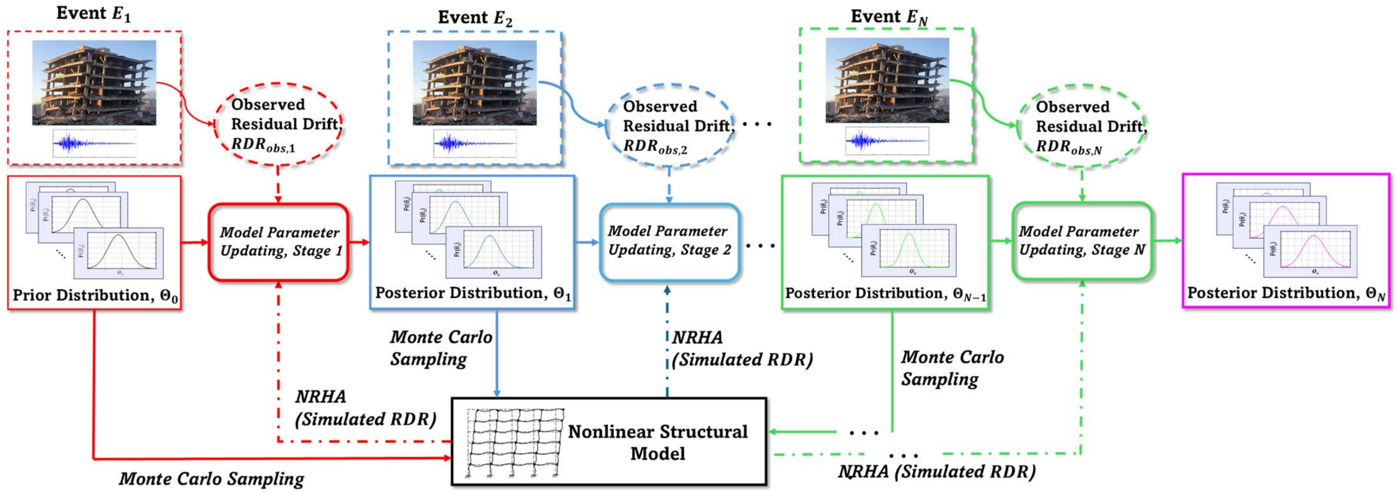

Fig. 1. Proposed framework for nonlinear model parameter updating under sequential seismic events.

sequential response history analysis under the back-to-back ground motions from E_1 and E_2.

Once the residual drift measurements following E_2 become available, the structural model parameters can be updated using $f_{\Theta_1}(\Theta_1)$ as the input, i.e., $f_{\Theta_2}(\Theta_2) = f_{\Theta_1}(\Theta_1|\mathrm{RDR}_{\mathrm{obs},2})$. Using these updated parameters, the sequential response history analysis under E_1 and E_2 can be repeated using $f_{\Theta_2}(\Theta_2)$ to obtain a new set of EDPs that are closer to the true distribution compared with that produced based on $f_{\Theta_1}(\Theta_1)$. This process can be repeated such that the EDP distribution under event sequence E_1 through E_i is initially obtained using the model parameters updated based on the response events from E_1 through E_{i-1} ($f_{\Theta_{i-1}}(\Theta_{i-1})$). This EDP distribution can then be further updated to include the residual drifts observed following event E_i, i.e., based on $f_{\Theta_i}(\Theta_i) = f_{\Theta_{i-1}}(\Theta_{i-1}|\mathrm{RDR}_{\mathrm{obs},i})$. The details of the model parameter updating procedure are presented in the next section, followed by a demonstration of the proposed framework using experimental data for a bridge pier subjected to a six-event ground motion sequence.

Mathematical Basis of the Model Parameter Updating

This section presents the mathematical basis of the model parameter updating procedure. To begin, we specify the vector $\Theta = (\theta_1, \theta_2, \theta_3, \ldots, \theta_n,)$ where θ_j represents the jth parameter that defines the nonlinear structural model, and n represents the number of considered parameters. Each parameter is described using a marginal probability distribution that is defined by some parametric or nonparametric functional form. This study adapts the procedure proposed by Yazgan (2009), which was originally developed for estimating peak story drift ratios using measured residual drifts. For a given model parameter or response demand, the parametric probability distribution is discretized into individual bins. In this approach, the various probability distributions defined in Eq. (1) are discretized into individual bins, and the updating is performed individually on each bin using the discrete form of Baye's theorem. The benefit of this approach is that it does not require that the various probability distributions (i.e., likelihood, prior, or marginal) to be parametric. However, once the updating procedure has been performed, the discrete probability distribution can be converted to a parametric form if needed.

To illustrate, consider the normally distributed model parameter, θ, which, as shown in Fig. 2, has been converted to an empirical distribution and represented using the histogram. Assuming that this represents the prior, each bin of the empirical distribution is treated as its own random variable. By defining the residual drift ratio (RDR) using a similar empirical distribution, the discrete form of Baye's rule is adopted as shown in Eq. (1)

$$P(\theta_k|\mathrm{RDR}_m) = \frac{P(\mathrm{RDR}_m|\theta_k)P(\theta_k)}{\sum_j P(\mathrm{RDR}_m|\theta_j)P(\theta_j)} = \frac{P(\mathrm{RDR}_m \cap \theta_k)}{P(\mathrm{RDR}_m)} \quad (1)$$

where θ_k and RDR_m = parameter of interest and residual drift ratio in the kth and mth bin of their respective empirical distributions. The posterior ($P(\theta_k|\mathrm{RDR}_m)$), prior ($P(\theta_k)$), likelihood ($P(\mathrm{RDR}_m|\theta_k)$), marginal ($P(\mathrm{RDR}_m)$), and joint ($P(\mathrm{RDR}_m \cap \theta_k)$) probabilities are also defined based on the individual bins that make up the empirical distributions of the different variables. The posterior probability of the model parameter conditioned on the observed residual drift ($\mathrm{RDR}_{\mathrm{obs}}$) can be expressed as shown in Eq. (2), using the total probability theorem

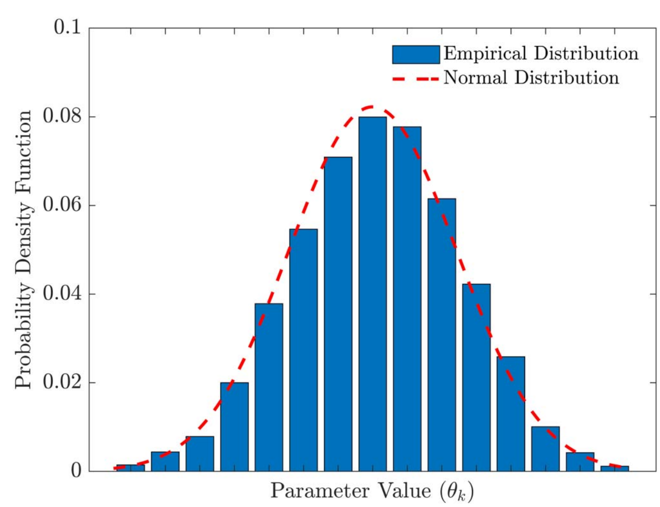

Fig. 2. Theoretical and empirical distributions where the latter is obtained by discretizing (or binning) the former.

$$P(\theta_k|\mathrm{RDR_{obs}}) = \sum_m P(\theta_k|\mathrm{RDR}_m \cap \mathrm{RDR_{obs}}) P(\mathrm{RDR}_m|\mathrm{RDR_{obs}}) \tag{2}$$

Eq. (2) can be simplified by recognizing that when the residual drift ratio within a specified bin (RDR_m) is known, θ_k is independent of $\mathrm{RDR_{obs}}$. In other words, these three parameters can be conceptualized as being part of a dependency chain ($\theta_k \rightarrow \mathrm{RDR}_m \rightarrow \mathrm{RDR_{obs}}$) where conditioning on RDR_m blocks the dependence between θ_k and $\mathrm{RDR_{obs}}$ (Pearl 2009). Therefore, Eq. (2) can be rewritten as follows:

$$P(\theta_k|\mathrm{RDR_{obs}}) = \sum_m P(\theta_k|\mathrm{RDR}_m) P(\mathrm{RDR}_m|\mathrm{RDR_{obs}}) \tag{3}$$

Combining Eqs. (1) and (3) produces

$$P(\theta_k|\mathrm{RDR_{obs}}) = \sum_m \frac{P(\mathrm{RDR}_m \cap \theta_k)}{P(\mathrm{RDR}_m)} P(\mathrm{RDR}_m|\mathrm{RDR_{obs}}) \tag{4}$$

where $P(\mathrm{RDR}_m \cap \theta_k)$ = probability that the simulated residual drifts exist within bin m (RDR_m) and the model parameter θ falls within bin k. As indicated in Eq. (1), this empirical joint probability is related to the likelihood function, $P(\mathrm{RDR}_m|\theta_k)$. For computing the marginal probability of the residual drift ratio in a specified bin ($P(\mathrm{RDR}_m)$), the joint probability ($P(\mathrm{RDR}_m \cap \theta_k)$) can be summed over θ_k such that

$$P(\mathrm{RDR_m}) = \sum_k P(\mathrm{RDR_m} \cap \theta_k) \tag{5}$$

Then, using Bayes theorem, $P(\mathrm{RDR}_m|\mathrm{RDR_{obs}})$ is computed as follows:

$$P(\mathrm{RDR}_m|\mathrm{RDR_{obs}}) = \frac{P(\mathrm{RDR_{obs}}|\mathrm{RDR}_m) P(\mathrm{RDR}_m)}{\sum_p P(\mathrm{RDR_{obs}}|\mathrm{RDR}_p) P(\mathrm{RDR}_p)} \tag{6}$$

The term $P(\mathrm{RDR_{obs}}|\mathrm{RDR}_m)$ depends on $P(\mathrm{RDR_{obs}})$, which is determined based on the uncertainty in the process used to measure the residual drift ratios. This issue is further discussed in the "Application of the Model Parameter Updating Framework" section.

Application of the Model Parameter Updating Framework

We implement the parameter estimation technique using experimental data for a RC bridge pier tested at the UCSD outdoor shake table. The specimen was subjected to six back-to-back ground motions without repair. This experiment is uniquely suited to demonstrating the proposed framework because of the sequential dynamic testing and presence of significant residual drifts. The uncertainty in the material parameters was considered by performing Monte Carlo-based response history analysis. For a given nonlinear structural model realization, the material parameters were sampled from their respective probability distributions. Initially, the central tendencies of the model parameter distributions (i.e., mean and/or median) were based on the expected values. Then, using the residual drift measurements from each event/record, the central tendency values were updated based on the maximum a posterior values from the Bayesian analysis.

Because the records from the sequential shake table testing were known and available, the uncertainty in the ground motion was not considered. The application scope of this study is the consideration of the structure being located close to a ground motion recording station such that the recorded motion from the station can be assumed to be similar for the structure. This may not be the case for some real-world applications. In other words, a ground motion recording will not always be available at the building site. As such, the issue of record-to-record variability is (in the "Conclusions" section) highlighted as a limitation of the study and an opportunity for future related work.

A nonlinear structural model of the bridge pier was first constructed based on expected parameter values. The uncertainties with respect to material model parameters as well as the modeling approach were considered. The next subsection summarizes the relevant details of the bridge pier experiment.

Overview of Bridge Pier Experiment

The structure considered was the RC bridge pier that was dynamically tested at the UCSD outdoor shake table. The pier was designed and constructed based on the Caltrans (2006) *Seismic Design Criteria*. The relevant experimental data were obtained from the DesignSafe (Rathje et al. 2017) repository. The test specimen comprised a column with a 1,220 mm (48 in.) diameter and a height of 7,315.2 mm (288 in. or 24 ft), which was attached to the shake table using a single isolated concrete footing. To simulate the superstructure mass, a large concrete block with a weight of 2,322 kN (522 kips) was mounted on top of the column. The column longitudinal reinforcement comprised 18 No. 11 ASTM A706 Grade 60 steel bars [35.8 mm/3.58 cm (1.41 in. diameter)] distributed uniformly around the circumference. The transverse reinforcement included two bundled No. 5 bars [15.88 mm/1.59 cm (0.625 in. diameter)] spaced at 152.4 mm/15.24 cm (6 in.) on center. In the experimental program, the bridge pier was subjected to a loading protocol that consisted of six sequential ground motions.

The characteristics of the ground motions used in the experiment are summarized in Table 1. Sourced from the Pacific Earthquake Engineering Research Institute (PEER) Next Generation Attenuation (NGA)-West2 (Bozorgnia et al. 2014) database, five of the records were from the 1989 Loma Prieta, California, earthquake (different recording stations) and one was from Kobe, Japan (1995). The records were selected based on a target spectrum for the hypothetical location in San Francisco. All of the Loma Prieta records were applied in their unscaled form, and a −0.8 scale factor was applied to the Kobe record. The magnitude of the recorded peak ground acceleration (PGA) ranged from $0.199g$ to $0.526g$ for the Loma Prieta records and $0.533g$ for the Kobe record.

The key response demand measurements from each record in the sequence are summarized in Table 2. Within the sequence, the first instance where significant residual deformation was observed was during EQ3, where peak and residual displacements of 360.68 mm (14.20 in.) and 63.25 mm (2.49 in.), respectively, were observed. This corresponded to drift ratios of 4.93% and −0.87%, respectively. As expected, the subsequent records (EQ4 and EQ5) also produced significant residual deformations. Specifically, EQ4

Table 1. Characteristics of ground motions used in the experimental program

Test	Earthquake	Station	Component	PGA (g)
EQ1	M 6.9 Loma Prieta	Agnew State Hospital	090	−0.199
EQ2	M 6.9 Loma Prieta	Corralitos	090	0.409
EQ3	M 6.9 Loma Prieta	LGPC	000	0.526
EQ4	M 6.9 Loma Prieta	Corralitos	090	0.454
EQ5	M 6.9 Kobe	Takatori	000	−0.533
EQ6	M 6.9 Loma Prieta	LGPC	000	−0.512

Table 2. Key response demand measurements from the experimental program

Test	Maximum displacement [mm (in.)]	Residual displacement [mm (in.)]	Ductility demand[a]
EQ1	61.98 (2.44)	0.762 (0.03)	1
EQ2	132.84 (5.23)	4.06 (0.16)	2
EQ3	360.68 (14.20)	−63.25 (−2.49)	4
EQ4	170.43 (6.71)	−59.18 (−2.33)	2
EQ5	568.96 (22.40)	104.40 (4.11)	8
EQ6	489.71 (19.28)	50.04 (1.97)	4

[a]Ratio of inelastic deformation to the yield deformation.

produced a residual displacement of −59.2 mm (−2.33 in. or −0.81% drift) and maximum displacement of 170.43 mm (6.71 in. or −2.33% drift). Due to the accumulation of damage, the EQ5 test saw the largest maximum and residual displacement of all the ground motions in the sequence at 568.96 mm (22.4 in. or 7.78% drift) and 104.4 mm (4.11 in. or 1.43% drift), respectively.

Nonlinear Structural Model Development

As shown in Fig. 3, the RC bridge pier was modeled as a two-dimensional (2D) planar structural system using OpenSeesPy version 3.5.1.10 (Zhu et al. 2018). There are three primary sources of uncertainty when probabilistically estimating the EDPs and damage using nonlinear structural response simulation. These include the uncertainty in the model parameters (e.g., such as the ones that are being updated), the input excitation, and the modeling approach. As mentioned previously, the model parameter uncertainty was explicitly considered using Monte Carlo-based structural response simulation. Whereas, assuming that the ground motions in the sequence are available (as was the case in this study), record-to-record uncertainty was not considered.

To minimize the uncertainty in the structural modeling approach, we evaluated several different strategies. The fiber element–based model (Alemdar and White 2005) was adopted because it is more suited [compared with the concentrated plastic hinge (Dides and de la Llera 2005)] to the aim of the study (Xiang et al. 2020; Su et al. 2020), which is to update the material parameters associated with

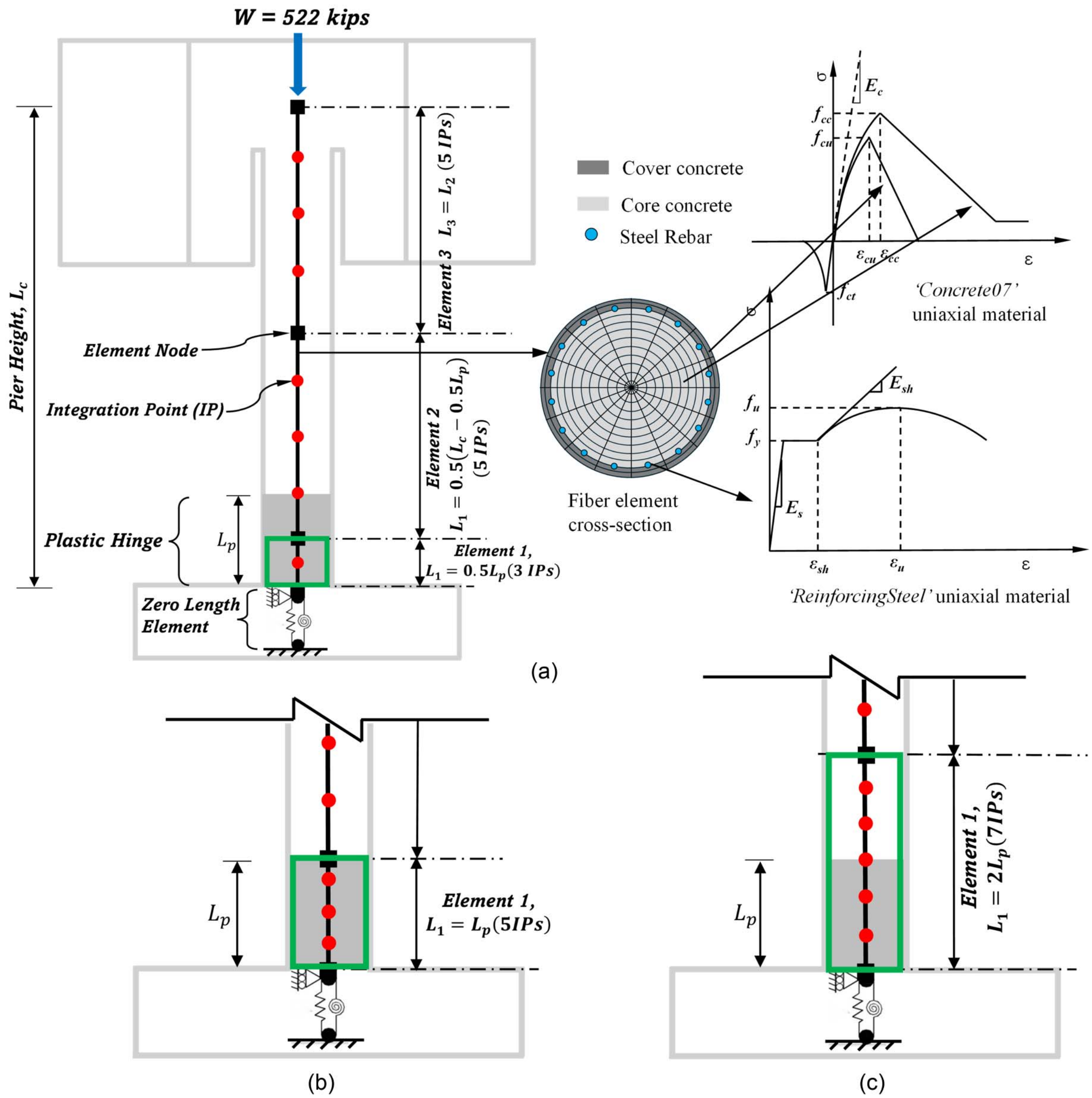

Fig. 3. Nonlinear structural model with DBC elements including variations in the length of the first element (L_1) as a function of the plastic hinge length (L_p): (a) $L_1 = 0.5L_p$; (b) $L_1 = L_p$; and (c) $L_1 = 2.0L_p$.

concrete and reinforcing steel. This is because the distributed plasticity formulation defines the nonlinearity based on the material stress–strain response. Whereas for the concentrated plasticity model, the inelastic behavior at member ends is characterized through phenomenological calibration of the observed force–deformation response.

Within this modeling paradigm, different strategies were evaluated, including the use of force-based (FBC) (Powell and Chen 1986) and displacement-based beam-column (DBC) (Taucer et al. 1991) elements, in addition to beam-with-hinge (BWH) (Scott and Fenves 2006) elements. The results of this evaluation showed that the DBC elements were most suitable for modeling the nonlinear response and strength degradation of this particular bridge pier case. As described subsequently in this section, the length of the base element (L_1) as a function of the plastic hinge length (L_p) was also considered as a source of uncertainty.

The fiber section was discretized by dividing the circular cross section into 10 radial and 20 circumferential segments. Uniaxial stress–strain material models were employed for concrete and steel with the nonlinear response captured in the material fibers. Within OpenSeesPy, the Concrete07 (Chang and Mander 1994) model and ReinforcingSteel (Dodd and Restrepo-Posada 1995) material models were used. Different compressive stress–strain relationships were used for the cover and core concrete fibers whereas, the same elastic modulus (E_c) and tensile parameters (e.g., tensile strength, f_{ct}) were used for the cover and core concrete fibers.

The steel cyclic behavior was governed by the buckling parameters β (amplification factor), r (buckling reduction factor), and γ (buckling constant), whose values were fixed at 1.0, 0.4, and 0.5, respectively, based on the recommendations of Gomes and Appleton (1997). The 2,322-kN superstructure weight was lumped at the topmost node where the column displacements were also measured. Strain penetration effects were captured using the Bond-SP01 (Zhao and Sritharan 2007) model. A zero-length element was defined near the column base with the rebar slip at yield (S_y) and ultimate strength (S_u) calculated using the expressions provided by Zhao and Sritharan (2007) with a pinching factor of $R = 0.5$. The length of the plastic hinge (L_p) was calculated per the guidelines provided by Priestley (1996).

The prior distributions of the steel and concrete model parameters are summarized in Tables 3 and 4. The distribution type and the values of the variables that define the probability model were based on the existing literature. Consistent with the recommendations of the Joint Committee of Structural Safety (JCSS) (JCSS 2001), the yield (f_y) and ultimate (f_u) steel strength, and ultimate strain (ε_u) were probabilistically represented as normally distributed random variables. All concrete strength and strain parameters were modeled using the lognormal distribution.

The mean values (μ) for steel and unconfined concrete parameters were selected based on their expected properties with the coefficients of variation (COVs) and corresponding standard deviation (σ) based on JCSS (2001). The elastic modulus parameters for steel (initial, E_s, and strain hardening, E_{sh}) and concrete (E_c) were modeled using the gamma distribution in accordance with Blondeel et al. (2018) and Liu and Shields (2017). The α and β parameters that define the gamma distribution were chosen such that they correspond to the expected elastic modulus [e.g., 206.8 GPa (30,000 ksi) for E_s and $57\sqrt{f'_c} \simeq 4,410$ ksi (30.4 GPa) for E_c]. All other parameters were modeled using the lognormal distribution based on prior studies (Haselton 2006; Melchers and Beck 2018). The mean value of f_{ct} was taken as $7.5\sqrt{f'_c} \simeq 0.6$ ksi (4.15 MPa) as suggested by Yassin (1994). A deterministic Rayleigh damping corresponding to 2.5% of critical (Segura et al. 2022) anchored to the first and third modes was specified.

The true or measured material property values for the longitudinal steel (No. 11 bars of ASTM A706) obtained from testing and reported in the experiment are summarized in Table 5, and the respective concrete properties are provided in Table 6. For the latter, the unconfined nominal strength (28-day) and the tested strength at 21, 29, and 43 days, were reported in the experimental documentation (Schoettler et al. 2012). The 43-day strain corresponding to the compressive strength and elastic modulus were also reported for unconfined concrete. The corresponding confined concrete properties were not documented. The reported measured properties will serve as a target in evaluating the effectiveness of the model parameter updating procedure.

Table 3. Prior distribution for reinforcing steel model parameters

Parameter	Distribution type	Distribution parameters
Yield strength, f_y (MPa)	Normal	$\mu = 465$, $\sigma = 33.41$
Ultimate strength, f_u (MPa)	Normal	$\mu = 608$, $\sigma = 41.8$
Elastic modulus, E_s (GPa)	Gamma	$\alpha = 266$, $\beta = 0.78$
Strain hardening modulus, E_{sh} (GPa)	Gamma	$\alpha = 19.25$, $\beta = 0.3$
Ultimate strain, ε_u	Normal	$\mu = 0.11$, $\sigma = 0.0055$
Strain at onset of hardening, ε_{sh}	Lognormal	$\mu_{\ln} = 0.007$, $\sigma_{\ln} = 0.25$

Note: $\mu_{\ln}$ = logarithmic mean; and $\sigma_{\ln}$ = logarithmic standard deviation.

Table 4. Prior distribution for concrete model parameters

Parameter	Distribution type	Distribution parameters
Unconfined concrete		
Compressive strength, f'_{cu} (MPa)	Lognormal	$\mu_{\ln} = 36$, $\sigma_{\ln} = 0.06$
Strain at f'_{cu} (ε_{uu})	Lognormal	$\mu_{\ln} = 0.0019$, $\sigma_{\ln} = 0.15$
Confined concrete		
Compressive strength, f'_{cc} (MPa)	Lognormal	$\mu_{\ln} = 50$, $\sigma_{\ln} = 0.06$
Strain at f'_{cc} (ε_{cc})	Lognormal	$\mu_{\ln} = 0.0038$, $\sigma_{\ln} = 0.20$
Confined and unconfined concrete		
Elastic modulus, E_c (GPa)	Gamma	$a = 30$, $\beta = 1.06$
Tensile strength, f_{ct} (MPa)	Lognormal	$\mu_{\ln} = 4.15$, $\sigma_{\ln} = 0.20$

Table 5. Mechanical properties of No. 11 ASTM A706 rebars reported in the experiment

Parameter	Values
f_y (MPa)	518.5
f_u (MPa)	706
E_s (GPa)	196
E_{sh} (GPa)	5.52
ε_y	0.0026
ε_u	0.122
ε_{sh}	0.011

Table 6. Mechanical properties of unconfined concrete reported in the experiment

Property	Values
Nominal strength (MPa)	27.6
21-day strength (MPa)	37.2
29-day strength (MPa)	40.0
43-day strength (MPa)	42.1
Elastic modulus, E_c (GPa) at 43 days	22.87
Strain at 43-day compressive strength, ε_{cu}	0.0026

Monte Carlo–Based Structural Response Simulation with Modeling Approach Uncertainty

Initially, the sequential structural response simulation was performed using the prior distribution model parameters documented in Tables 3 and 4. To consider the uncertainty in the nonlinear structural model parameters, a Monte Carlo–based procedure was adopted. Specifically, for a given realization, each model parameter was sampled and used to generate a nonlinear structural model of the bridge pier. During sampling, some important fundamental constraints were applied to the relative values of specific model parameters. For the steel properties, the ratio of ultimate to yield strength (f_u/f_y) was limited within the range 1.1 to 1.5. Similarly, the ratio of the strain hardening modulus to the elastic modulus (E_{sh}/E_s) was limited to 0.005 to 0.05. The strain at the onset of hardening (ε_{sh}) was constrained to be greater than the yield strain (ε_y) and less than the ultimate strain (ε_u), i.e., $\varepsilon_y < \varepsilon_{sh} < \varepsilon_u$. For concrete, the confined compressive strength (f'_{cc}) was always greater than that of the unconfined concrete (f'_{cu}). The same constraint is applied to the corresponding strain values, i.e., $\varepsilon_{cc} > \varepsilon_{cu}$. These constraints ensured that the sampled parameter values do not produce unrealistic fiber stress–strain curves.

The uncertainty in the length of the first element at the column base (L_1) was varied as a multiple of the plastic hinge length (L_p). This was achieved by specifying the following three values for the first element length: $L_1 = 0.5L_p$ [Fig. 3(a)], $L_1 = L_p$ [Fig. 3(b)], and $L_1 = 2L_p$ [Fig. 3(c)]. The value of L_1 has implications to the integration scheme performed during the analysis. For $L_1 = 0.5L_p$, the base element had three integration points, whereas for $L_1 = L_p$ and $L_1 = 2L_p$, the base element had five and seven integration points, respectively.

Three sets of 1,500 Monte Carlo–based structural model realizations were generated. The random model parameter samples were obtained from their theoretical prior distributions by employing the inverse method. The sampled parameters were then grouped into histogram bins. Each of the 1,500 realization sets corresponded to one of the three L_1 values. The 1,500 realizations for each L_1 value were justified based on a convergence analysis of the EDP statistics (i.e., the effect of the number of realizations on the probability distributions of the generated EDPs). Therefore, a total of 4,500 realizations were considered for the structural response estimation with material parameter uncertainty.

Since L_p is function of some model parameters, its value was also varied accordingly for each realization. Thus, the first element length L_1, which is a function of L_p, was also different for every realization. For each realization, sequential nonlinear response history analysis (NRHA) was performed with the ground motions used in the experiment. For practical purposes, the implicit assumption here was that the ground motions are available at or near (within reason) the site of interest within a reasonable timeframe following the earthquake. The limitations of this assumption are discussed in the conclusion along with suggestions for future related work.

The NRHA was conducted using the implicit Newmark-beta average acceleration time integration method (Newmark 1959), which is unconditionally stable. Within each time step, the Newton–Raphson iterative algorithm (Chopra 1995) was employed for convergence. The time step for the analyses (Δt) was taken to be same as that of the sampling step size of the ground motion series. The first five ground motions were considered for the sequential analysis; however, the model updating was only performed following the third, fourth, and fifth records because the first two produced negligible residual drifts. The fact that model parameter updating can only be performed in the presence of measurable significant residual drifts may be considered a limitation. However, as discussed in the "Introduction," the envisioned context is a noninstrumented building, which implies that the entire response history is unavailable. For a given sequential analysis realization, each ground acceleration time series is appended with 30 s of zero padding to allow the system to come to rest following the shaking (Raghunandan et al. 2015).

Sequential Response History Analysis Results Based on the Prior Distribution Model Parameters

Fig. 4 shows the empirical distribution of the residual [Fig. 4(a)] and maximum [Fig. 4(b)] drift under EQ3 when the nonlinear structural model was constructed based on the prior distribution parameters given in Tables 3 and 4. The histogram probabilities have been normalized such that the vertical axes correspond to probability density function (PDF) values. The histograms also show the observed values from the experiment. For the residual drift, the mean simulated value (0.86%) was almost exactly the same as the value observed from the experiment (0.87%). However, the median (0.78%) and mode (0.68%) of the simulated residual drift distribution were approximately 12% and 21% less than the observed value, respectively.

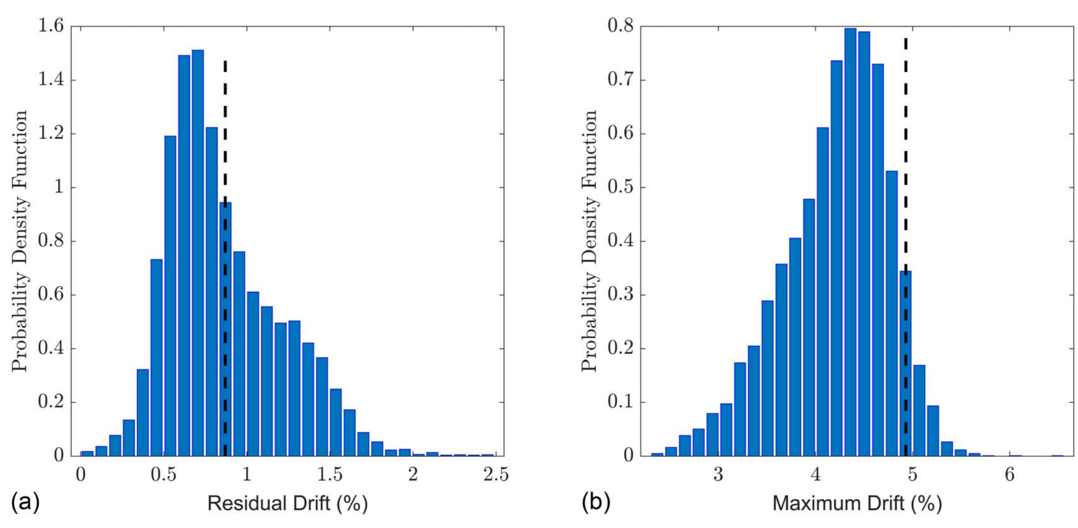

Fig. 4. Empirical distribution of the simulated: (a) residual; and (b) maximum drifts under EQ3.

The coefficient of variation for the residual drift was 0.4. The mean simulated peak drift was approximately 17% less than the value observed in the experiment (4.93%). Unlike the residual drift histogram which had a left-skewed or lognormallike shape, the peak drift empirical distribution had a right-skewed shape. As a result, the median (4.3%) and mode (4.4%) of the simulated peak drift were greater than and closer to the observed value compared with the mean (the reverse is true for the residual drift). Yet, the median and mode peak drifts were still measurably less (11%–13%) than the observed values.

Model Parameter Updating

As mentioned previously, whereas the six-record sequence was considered in the response history analyses, the structural model parameters were only updated after the third, fourth, and fifth ground motions. For this purpose, the empirical joint distribution of the sampled prior parameters and the residual drift from the response history analysis are necessary. In other words, $p_{\Theta,\mathrm{RDR}}(\theta, rdr)$ is needed where θ represents the model parameter of interest and rdr is the residual drift from the NRHA.

Fig. 5 shows the empirical joint distribution of the yield (f_y) [Fig. 5(a)] and ultimate (f_u) [Fig. 5(b)] strengths of steel, and the residual drifts obtained from NRHA under the ground motion sequence up to EQ3. Within a given bin, the horizontal axes values represent RDR_m and θ_j [e.g., $f_{y,j}$ in Fig. 5(a)], and the vertical axis value corresponds to $P(\theta_j \cap \mathrm{RDR}_m)$ [e.g., $P(f_{y,j} \cap \mathrm{RDR}_m)$ in Fig. 5(a)]. For the choice of the number of bins, a sensitivity analysis was conducted where the maximum a posteriori (MAP) estimate (bin center value having maximum probability) after updating did not vary by more than 5% after the number of bins was incrementally increased. Based on this consideration, 15 bins were found to be sufficient for all parameters except the elastic modulus. A total of 20 bins were used for E_s and E_c, and 15 bins were used for the remaining parameters. Similar joint distributions were developed for all the model parameters given in Tables 3 and 4.

To evaluate Eq. (6), the probability of the observed or measured residual drift ($\mathrm{RDR_{obs}}$) conditioned on the simulated residual drift value in bin m (RDR_m) is needed, i.e., $P(\mathrm{RDR_{obs}}|\mathrm{RDR}_m)$. This requires $\mathrm{RDR_{obs}}$ to be defined in terms of a probability distribution. In the experimental setup, the relative horizontal displacement between the shake table and the column was measured using cable-extension position transducers, known commercially as spring potentiometers. Data regarding the accuracy and precision of the instruments used in the experiment were not reported. Therefore, as a best estimate, the precision or repeatability of commercially available moderate range potentiometers was used, which is $\pm 0.05\%$ of the full-scale (FS) or measurable range (Intertechnology 2024).

Given this information, and assuming the residual drift measurements are normally distributed about the measured value from the experiments, the corresponding standard deviation ($\sigma_{\mathrm{RDR_{obs}}}$) was computed as follows:

$$\sigma_{\mathrm{RDR_{obs}}}(\%) = \left(\frac{0.05\% \cdot \mathrm{FS}}{L_c}\right) \cdot 100 \qquad (7)$$

where L_c = height of the pier; and FS = full-scale range of the potentiometer. Eq. (7) assumes that 68% of the measurement values lie within $\mu_{\mathrm{RDR_{obs}}} \pm \sigma_{\mathrm{RDR_{obs}}}$.

The full-scale range based on the moderate range potentiometer was taken to be 100 in. (Intertechnology 2024). By taking the mean of the observed residual drift as the value measured during the experiment (or in the field in real applications) and the standard deviation

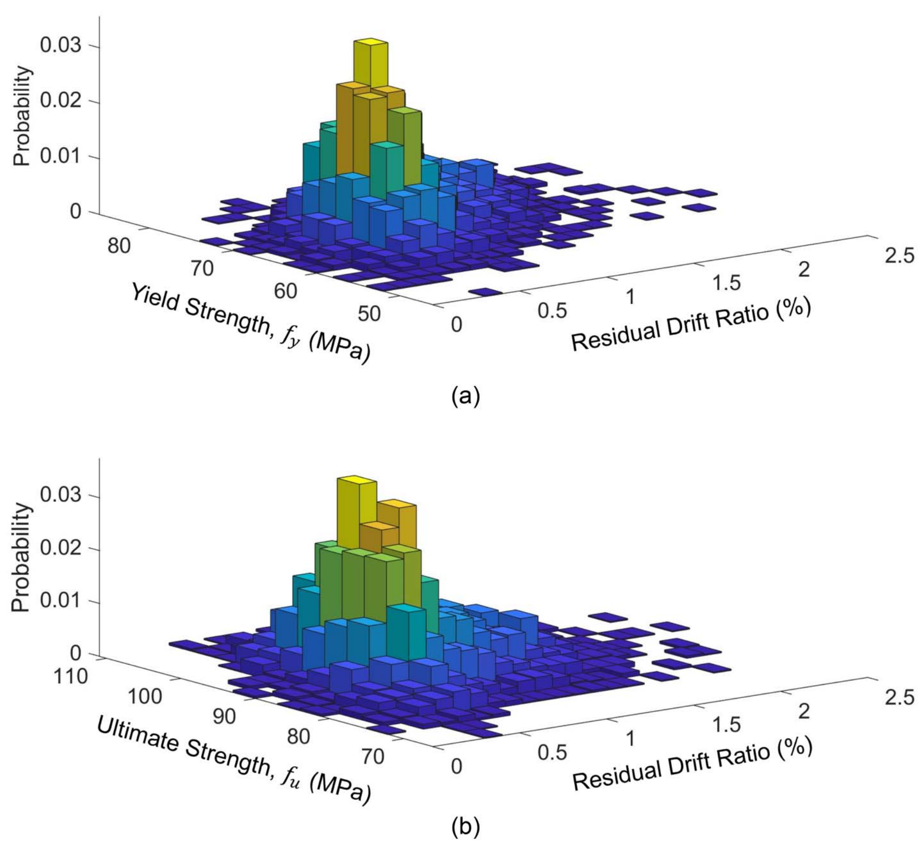

Fig. 5. Empirical joint probability distribution of (a) the steel yield strength and residual drift; and (b) the steel ultimate strength and residual drift.

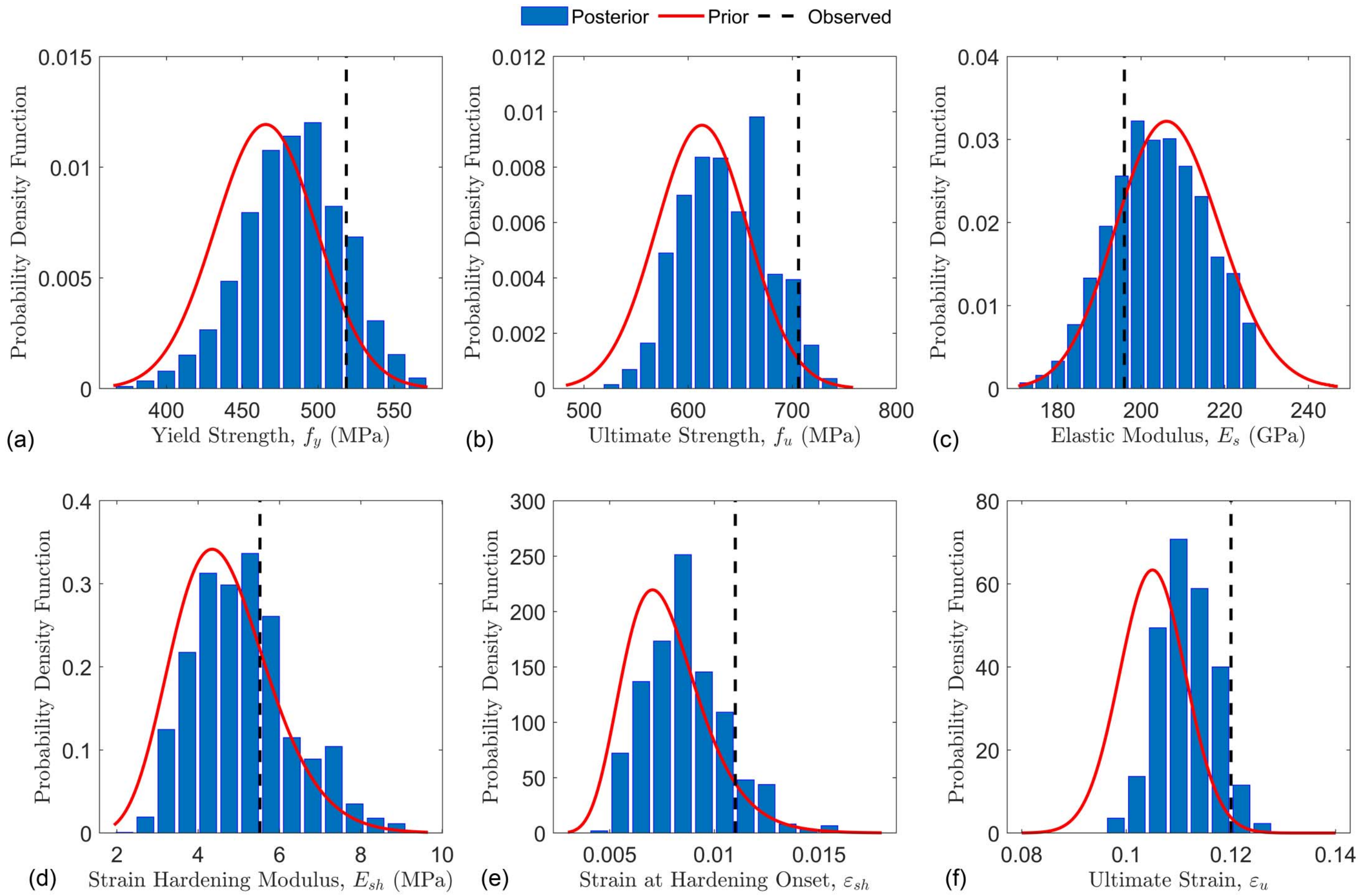

Fig. 6. Prior and post-EQ3 posterior probability distributions along with the true values of the steel model parameters: (a) f_y; (b) f_u; (c) E_s; (d) E_{sh}; (e) ε_{sh}; and (f) ε_u.

computed in Eq. (7), the normally distributed $\mathrm{RDR}_{\mathrm{obs}}$ was discretized into the same number of bins as the NRHA-based residual drift under the considered ground motion in the sequence. For a given bin, the empirical joint probability of the observed and simulated residual drift was then normalized by the marginal probability of the latter to obtain the conditional probability, i.e., $P(\mathrm{RDR}_{\mathrm{obs}}|\mathrm{RDR}_m) = [P(\mathrm{RDR}_{\mathrm{obs}} \cap \mathrm{RDR}_m)]/P(\mathrm{RDR}_m)$. Finally, the updated or posterior bin-specific model parameter probability was computed using Eq. (5).

Post-EQ3 Model Parameter Updating Results

The detailed results of the model parameter updating following the third ground motion in the sequence is presented in this subsection. The results for the other two ground motions in the sequence (fourth and fifth) are summarized in the next subsection. Fig. 6 compares the prior and posterior distributions of the steel parameters. Overall, the comparison showed appreciable updates in the distributions of all the parameters. Moreover, relative to the prior, the location of the posterior distribution was closer to the values reported in the experiment.

This observation also applies to the concrete parameters, whose prior and posterior distributions are shown in Fig. 7. For each posterior empirical distribution, the MAP estimate (i.e., the bin value corresponding to the maximum probability) was taken as the updated mean value of the parameter. The parameter value for a given bin was taken as the average of the bounding edges for that bin. For comparison, Table 7 summarizes the prior mean, posterior MAP, and the measured or observed value of the steel and concrete parameters reported in the experiment. The percent errors for the prior and posterior means relative to the observed parameter values are also presented.

As evidenced by the comparison of the percent errors based on the prior and posterior, significant improvement in the mean approximation of the model parameters was observed. For steel, the mean prior strength parameters were roughly 10%–15% lower than the measured values. For the posterior, the same parameters were approximately 4%–5% lower than the measured values. The prior means for the strain at the onset of hardening and the corresponding modulus were significantly lower than the measured values (22% and 36%, respectively). However, the percent errors were reduced by factors of approximately 7 and 1.6, respectively, after the updating. The prior mean of the elastic modulus was only 5.5% lower than the measured value. Still, this percent error was significantly reduced (to 1.5%) after the updating. The ultimate strain had the smallest change in the percent error between the prior and posterior.

For the concrete parameters, measured values were only available for the strength, modulus and ultimate strain of the unconfined concrete. Relative to the posterior, the unconfined ultimate strength had a more than 10-fold reduction in the prior percent error. The reduction for the elastic modulus of concrete was not as significant compared with the corresponding steel modulus. However, the reduction in percent error due to updating for the ultimate strain was comparable for concrete and steel.

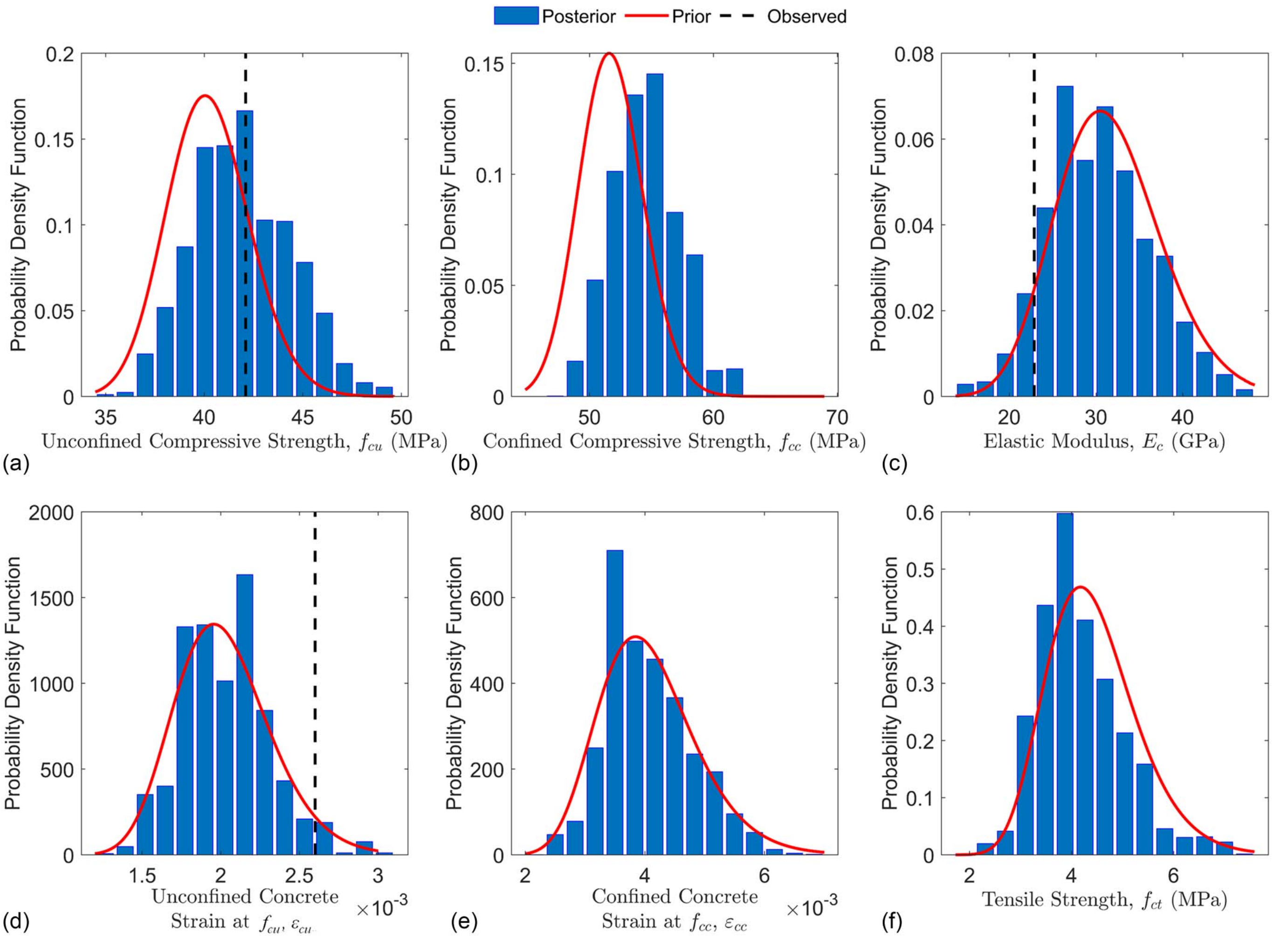

Fig. 7. Prior and post-EQ3 posterior probability distributions along with true values of the concrete model parameters: (a) f_{cu}; (b) ε_{cu}; (c) E_c; (d) f_{cu}; (e) ε_{cc}; and (f) f_{ct}.

Fig. 8 compares the response history of the bridge pier drift, and the base moment–curvature response based on the prior and posterior mean model parameters to the response recorded during the experiment. Notably, the overall response history [Fig. 8(a)] based on the updated model parameters was closer to that of the experiment. The response based on the prior parameters was significantly different from the experiment. As summarized in Table 8, the peak and residual drifts were approximately 40% and 50% less than the corresponding experimental values. Whereas for the response based on the posterior mean parameters, the simulated peak and residual drifts were less than 5% and less than 15% lower than the experimental values, respectively. Similarly, relative to the response based on the prior, the ability to capture the base moment–curvature response [Fig. 8(b)] was significantly improved when the posterior parameters were used in the analysis.

Model Parameter Updating Results for the Full Sequence

The post-EQ3 model parameter updating procedure was also applied (sequentially) following the EQ4 and EQ5 ground motions. Fig. 9 compares the percent errors of the posterior parameter estimates following the post-EQ3, post-EQ4, and post-EQ5 updating. Except for ε_u, there was a reduction in the percent error of the steel model parameters after each successive ground motion in the sequence. In other words, as we transitioned from EQ3 to EQ4 and EQ5, the updated model parameters became closer to the true or measured values. In some cases (e.g., f_y, f_u, and ε_{sh}), the movement toward the true value was gradual. For others (e.g., E_{sh}), there was significant movement between EQ3 and EQ4 and very little from EQ4 to EQ5.

For ε_u, the percent error did not change between EQ4 and EQ5. Whereas for E_{sh}, the change in percent error was minimal from EQ3 to EQ4 but much more significant from EQ4 to EQ5. The observations for the concrete modeling parameters were generally similar. For E_c, there was a gradual transition toward the true parameter value, whereas most of the reduction in percent error for ε_{cu} happened between EQ3 and EQ4.

Fig. 10 compares the postupdate percent error for the simulated residual and peak drifts. For the residual drift, there was a significant drop between EQ3 and EQ4 then a slight uptick following EQ4. The simulated peak drift also trended toward the observed value between EQ3 and EQ5. Between EQ4 and EQ5, there was a significant increase in the percent error, however, the final simulated value was still within 10% of the true value.

Parametric Sensitivity Analysis

The ability of the model parameter updating procedure to improve the accuracy of the structural response simulation depends on two

Table 7. Comparing the prior and posterior mean to the reported or measured parameter values

Parameter	Prior mean	MAP estimate	Measured value	Prior percent error (%)	Posterior percent error (%)
			Steel parameters		
f_y (MPa)	465	496.4	518.5	10.2	4.3
f_u (MPa)	607	668.8	706	14.1	5.3
E_s (GPa)	206.8	198.91	195.99	5.5	1.5
E_{sh} (GPa)	4.2	5.34	5.52	23.9	3.13
ε_{sh}	0.007	0.0085	0.011	36.4	22.7
ε_u	0.105	0.11	0.12	12.5	8.33
			Concrete parameters		
f_{cu} (MPa)	37.2	42.1	42.1	11.5	0.0
f_{cc} (MPa)	51.5	55.8	N/A	N/A	N/A
ε_{cu}	0.0019	0.0022	0.0026	26.9	15.4
ε_{cc}	0.0038	0.0035	N/A	N/A	N/A
E_c (GPa)	30.4	26.2	22.87	32.6	14.5
f_{ct} (MPa)	4.15	3.86	N/A	N/A	N/A

Note: N/A = measured values are not available, i.e., not reported in experiment.

Table 8. Comparing the simulated peak and residual drifts based on the prior and posterior parameters to the experimental values (after EQ3 updating)

EDP	Simulated using prior mean model parameters (%)	Simulated using MAP estimates of the model parameters (%)	True value (%)	Prior error (%)	Posterior error (%)
Residual drift	−0.45	−0.75	−0.87	48.3	13.8
Maximum drift	−3.11	−4. 78	−4.93	36.92	3.04

factors. The first is the extent to which the updating procedure shifts the distribution of the parameter toward the true or measured value. The results presented in Figs. 6 and 7 showed that this varied significantly across the different parameters. This variation is reflected in both the degree to which the location (i.e., mean) of the distribution moves as well as the final location of the posterior relative to the measured parameter value.

The second factor is the sensitivity of the response demands produced by the NRHA to variations in the parameter of interest. For instance, if a parameter is shown to have negligible influence on the response demands, the extent to which the distribution is affected by the updating procedure is less important. On the other hand, for parameters that are known to be highly influential to the response demands generated by the structural response simulation, more emphasis should be placed on how their distributions are affected by the updating procedure. The results presented previously address the first factor, i.e., the extent to which the updating procedure affects a given parameter. The second factor is addressed in this section through a sensitivity analysis to evaluate which of the parameters are most influential to the response demands.

The sensitivity analysis was performed by systematically and incrementally varying the value of each parameter within some upper and lower bound while the others were held constant, then assessing the change in the peak and residual drift demands from the structural response simulation. Given the large number of parameters, the computational demand required for this process was reduced by constructing a surrogate model that estimated the response demands as a function of the structural model parameters. For this purpose, the Extreme Gradient Boosting (XGBoost) machine learning model (Chen and Guestrin 2016) was utilized. The XGBoost model is a widely used ensemble machine learning algorithm that leverages gradient boosting. It operates by sequentially constructing decision trees, with each tree in the sequence aiming to correct the prediction errors of the previous one by minimizing the squared error loss function.

Given the use case of the surrogate model (sensitivity analysis), less focus was placed on maximizing accuracy. Instead, the goal was to have a trained model that provides reasonable predictive performance. With that in mind, the following hyperparameter values were chosen: 1,000 estimators, learning rate of 0.05, maximum depth of each tree of 7, and minimum sum of instance weights of 1. Because the model was not intended for use beyond the current study, generalization was not a concern. Therefore, the entire data set was used for training.

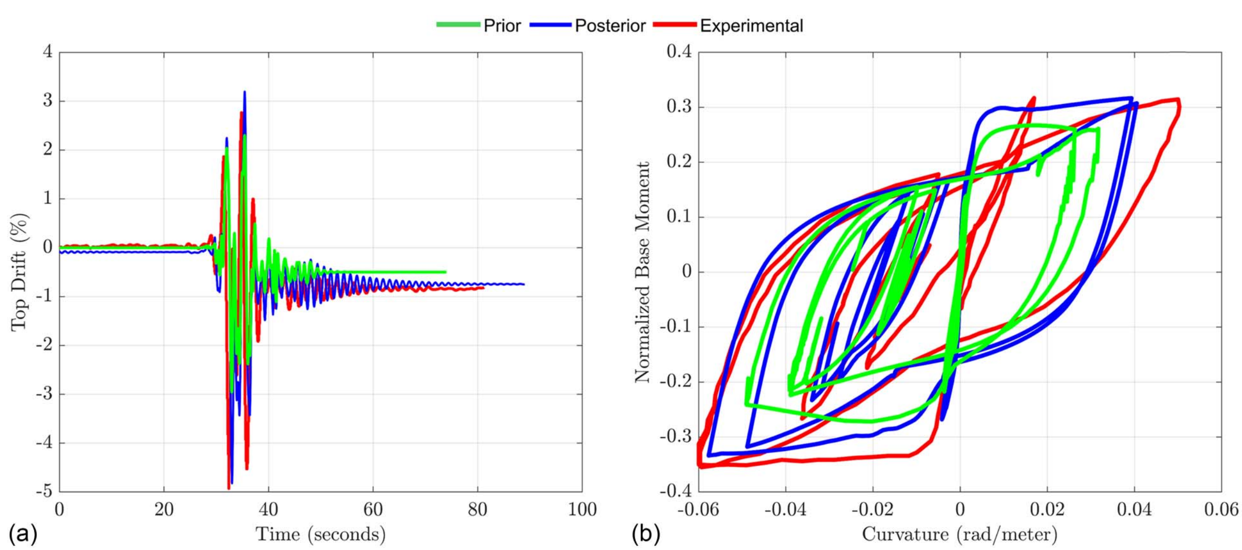

Fig. 8. Comparing the simulated (based on prior and posterior parameters) and experimental response under EQ3: (a) response history; and (b) normalized (by seismic weight times column height) base moment versus curvature.

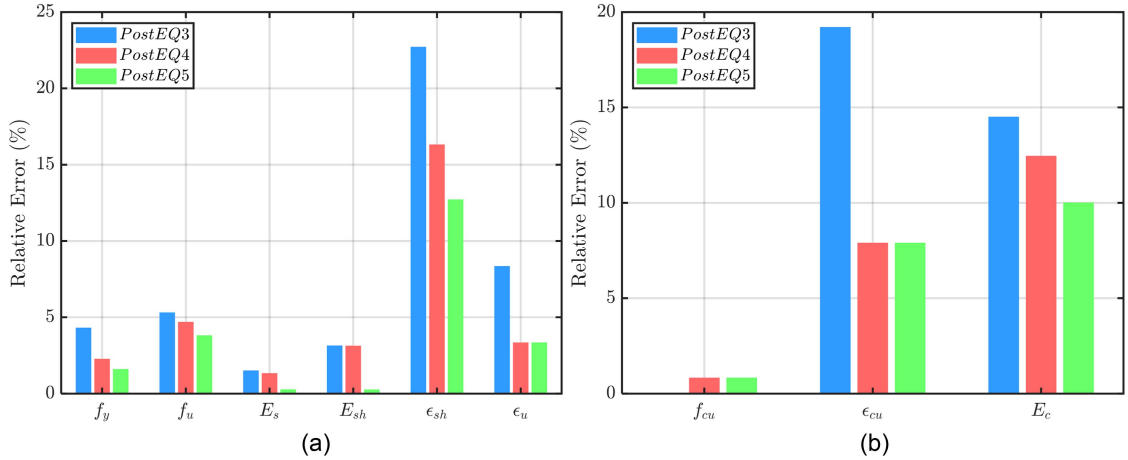

Fig. 9. Percent errors in the model parameter estimates for (a) steel; and (b) concrete after updating.

The XGBoost model was trained using the data generated by the Monte Carlo-based response estimation. One model was developed for each ground motion in the sequence (only the ones considered in the updating) using the sampled model parameters as the inputs and the peak and residual drift demands as the output. The performance of the models were evaluated using the coefficient of determination (R^2). All six models (two for each ground motion times three ground motions, i.e., EQ3, EQ4, and EQ5) produced R^2 values that were greater than or equal to 0.97, which was deemed fit for purpose.

The sensitivity of the response demands to the input parameters was evaluated using partial dependency plots (PDPs). For a given parameter of interest, the value was varied incrementally while the others were held to their MAP estimate. Then, the XGBoost models were used to estimate the peak and residual drifts. Figs. 11 and 12 show PDPs for steel and concrete parameters, respectively, for the case where the structure is subjected to EQ3. The horizontal and vertical axes are normalized by the respective mean values of the model parameters and response measure.

From Fig. 11(a), we can observe that among the six steel parameters, the residual drift was most sensitive to the strength parameters (f_y and f_u), with f_y having the greatest influence. Also, there was a positive correlation between the residual drift and the two strength parameters. The strain hardening modulus and strain corresponding to the onset of hardening also had a measurable influence on the residual drift. However, the correlation with the residual drift was positive for E_{sh} and negative for ε_{sh}. In other words, the residual drift increased as the strain hardening ratio increased but decreased as the strain corresponding to the onset of hardening increases. The steel elastic modulus and ultimate strain had a minimal impact on the residual drift.

For the maximum drift [Fig. 11(b)], the elastic modulus was by far the most influential steel parameter. The correlation between these two parameters was also negative, which means that higher E_s values reduce the peak drift. The yield strength, which is the next most influential steel parameter, was also negatively correlated with the maximum drift. The other three parameters (f_u, E_{sh}, and ε_u) appeared to have a minimal impact on the maximum drift.

Among the concrete parameters shown in Fig. 12, the residual drift was most sensitive to the tensile strength (f_{ct}) with which it

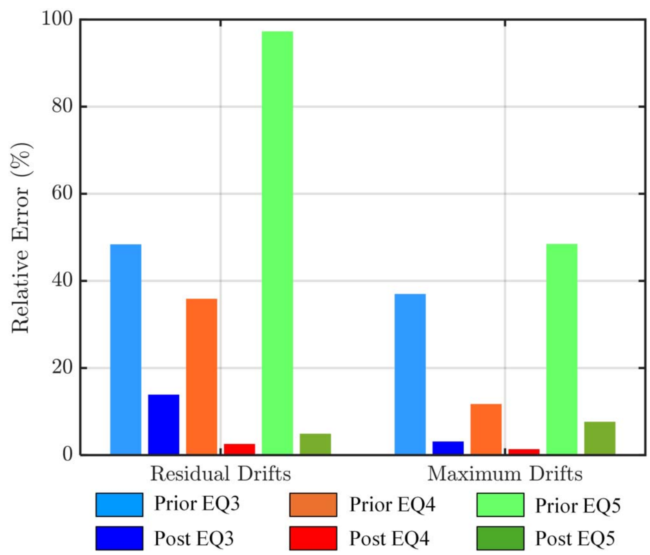

Fig. 10. Comparison of percent errors of the residual and maximum drifts simulated using prior and posterior means of the model parameters.

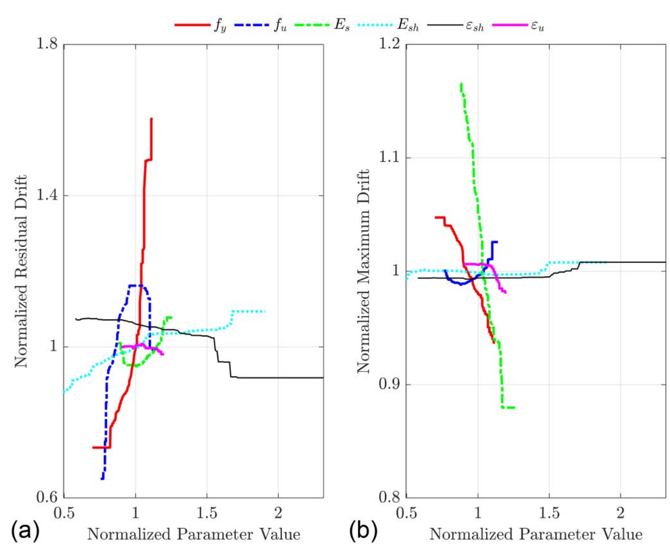

Fig. 11. PDPs for steel model parameters when the structure was subjected to the EQ3 ground motion.

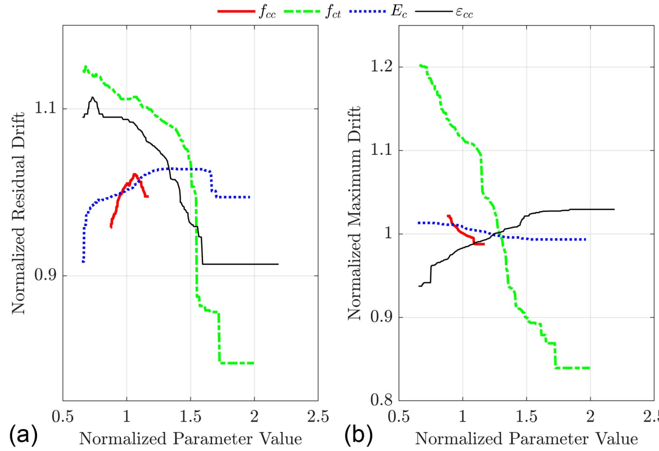

Fig. 12. PDPs for concrete model parameters when the structure was subjected to the EQ3 ground motion.

has a strong negative correlation. The f_{ct} also had the greatest influence on the peak drift and like the residual drift, the sign of the correlation was negative. The strain corresponding to peak strength of the confined concrete was negatively correlated with the residual drift but the correlation with the peak drift was positive. For peak drifts, increasing ε_{cc} corresponded to more ductile concrete behavior, which produced more inelastic deformations and hence the positive correlation. For residual drifts however, the direction of the trend with ε_{cc} was reversed because confined concrete allows gradual and stable postpeak strength degradation, which corresponds to higher recentering capability. Thus, with higher ε_{cc}, the residual drift demand decreases. The other two parameters (f_{cc} and E_c) had only a modest effect on both demand parameters.

Conclusions

When coupled with in-person inspections and field measurements, nonlinear structural modeling and simulation can be used to inform critical decisions about the safety and functionality of infrastructure in the postearthquake environment. Model parameter updating based on response measurements have been shown to be effective for improving the accuracy of structural response simulations. Although a structure that is not instrumented will have no record of the response history, new technologies such as LiDAR and unmanned aerial vehicle mounted devices can be used to measure residual deformations after the ground shaking has subsided. It is within this context that this paper proposed a nonlinear structural model parameter estimation methodology that utilizes only residual drift measurements from sequential seismic events.

For a structure that undergoes repeated shaking from back-to-back earthquakes, the nonlinear structural model is updated after each event using residual drift measurements. The framework is demonstrated using experimental data from a bridge pier tested at the UCSD outdoor shake table. The pier was subjected to a sequence of six ground motions and had significant residual drift demands, making it an ideal testbed for evaluating the effectiveness of the model parameter updating procedure.

A Bayesian framework was used to update the concrete and steel model parameters that are used as inputs into the nonlinear structural model. The updates were performed over a three-ground-motion sequence where for each record, the observed residual drift was used as the basis of the updating. The uncertainty in the model parameters was considered by performing sequential nonlinear response history analysis using both the prior and posterior distributions. The MAP value of the model parameter distribution was then used in a deterministic analysis where the simulated and measured responses were compared. The results showed the updating procedure produced significant incremental (i.e., from one ground motion to the next in the sequence) shifts in the MAP estimates toward the measured values for both the steel and concrete parameters.

This then resulted in considerable reductions in the difference between the simulated and measured values of the peak and residual drift. For example, the prior distribution parameters produced an approximately 50% difference between the simulated and measured residual drift in the first record of the sequence. This difference was reduced to approximately 5% when the MAP parameter values obtained following the third record in the sequence was used.

Similarly, the error for the peak drift was reduced from approximately 40% for the prior parameter values to less than 10% when the MAP was used. The results from a sensitivity analysis showed that the model parameters that had the most influence on the response varied based on the material. For steel, the yield strength dominated the residual drift demand whereas the elastic modulus had the greatest influence on the maximum drift. Whereas for concrete, the tensile strength dominated the response for both demand parameters. However, the strain corresponding to peak confined compressive strength was also a major influence with opposite correlations with the residual and peak drifts.

Overall, this study advances the use of structural response simulation to guide decision-making in the postearthquake environment by establishing a framework for model parameter updating based only on residual drift measurements. Although the proposed framework was developed to be agnostic to the type of structure, a single application context that considers the response of bridge piers to sequential ground motions was considered. Therefore, additional studies are needed to evaluate its effectiveness for other types of structures (e.g., buildings). Also, the effect of record-to-record uncertainty was not considered in this study because the ground motions used in the experiment were accessible.

The underlying assumption of this study is that the structure is located close to a ground motion recording station such that the motion affecting its site can be assumed to be similar to that recorded in the station. In a real-world postearthquake application context, the ground motions at the site of interest may not be available. Therefore, future work in this area should assess the extent to which record-to-record uncertainty affects the updating procedure. Lastly, the fidelity and accuracy of the prior model may have implications to the effectiveness of the updating procedure. For example, if the prior model parameters deviate too far from the true value, this may limit the efficacy of the updating procedure. This issue should be investigated in subsequent studies.

Data Availability Statement

Some or all data, models, and codes that support the findings of the study are available from the corresponding author upon reasonable request.

Acknowledgments

The research presented in this paper was supported by the National Science Foundation CMMI Research Grant No. 2242767.

Author Contributions

Budhaditya De: Conceptualization; Data curation; Formal analysis; Investigation; Methodology; Software; Validation; Visualization; Writing – original draft. Henry V. Burton: Conceptualization; Funding acquisition; Investigation; Project administration; Resources; Supervision.

References

Alemdar, B. N., and D. W. White. 2005. "Displacement, flexibility, and mixed beam–column finite element formulations for distributed plasticity analysis." *J. Struct. Eng.* 131 (12): 1811–1819. https://doi.org/10.1061/(ASCE)0733-9445(2005)131:12(1811).

Allali, S. A., M. Abed, and A. Mebarki. 2018. "Post-earthquake assessment of buildings damage using fuzzy logic." *Eng. Struct.* 166 (Jul): 117–127. https://doi.org/10.1016/j.engstruct.2018.03.055.

Astroza, R., H. Ebrahimian, Y. Li, and J. P. Conte. 2017. "Bayesian nonlinear structural FE model and seismic input identification for damage assessment of civil structures." *Mech. Syst. Signal Process.* 93 (Sep): 661–687. https://doi.org/10.1016/j.ymssp.2017.01.040.

Blondeel, P., P. Robbe, G. Lombaert, and S. Vandewalle. 2018. "Multilevel Monte Carlo for uncertainty quantification in structural engineering." Preprint, submitted August 31, 2018. https://arxiv.org/abs/1808.10680.

Bozorgnia, Y., et al. 2014. "NGA-West2 research project." *Earthquake Spectra* 30 (3): 973–987. https://doi.org/10.1193/072113EQS209M.

Caltrans. 2006. *Seismic design criteria v1.4*. Sacramento, CA: Caltrans.

Chang, G. A., and J. B. Mander. 1994. *Seismic energy based fatigue damage analysis of bridge columns. Part I: Evaluation of seismic capacity.* Technical Rep. No. NCEER-94-0006. Buffalo, NY: National Center for Earthquake Engineering Research.

Chen, T., and C. Guestrin. 2016. "XGBoost: A scalable tree boosting system." In *Proc., 22nd ACM SIGKDD Int. Conf. on Knowledge Discovery and Data Mining*, 785–794. New York: Association for Computing Machinery. https://doi.org/10.1145/2939672.2939785.

Chopra, A. K. 1995. *Dynamics of structures: Theory and applications to earthquake engineering. Prentice-Hall international series in civil engineering and engineering mechanics*. London: Pearson Education.

Conde, B., L. F. Ramos, D. V. Oliveira, B. Riveiro, and M. Solla. 2017. "Structural assessment of masonry arch bridges by combination of non-destructive testing techniques and three-dimensional numerical modelling: Application to Vilanova Bridge." *Eng. Struct.* 148 (Oct): 621–638. https://doi.org/10.1016/j.engstruct.2017.07.011.

Dai, K., J. Wang, B. Li, and H. P. Hong. 2017. "Use of residual drift for post-earthquake damage assessment of RC buildings." *Eng. Struct.* 147 (Sep): 242–255. https://doi.org/10.1016/j.engstruct.2017.06.001.

De Domenico, D., D. Messina, and A. Recupero. 2022. "Quality control and safety assessment of prestressed concrete bridge decks through combined field tests and numerical simulation." *Structures* 39 (May): 1135–1157. https://doi.org/10.1016/j.istruc.2022.03.086.

Dides, M. A., and J. C. de la Llera. 2005. "A comparative study of concentrated plasticity models in dynamic analysis of building structures." *Earthquake Eng. Struct. Dyn.* 34 (8): 1005–1026. https://doi.org/10.1002/eqe.468.

Dodd, L. L., and J. I. Restrepo-Posada. 1995. "Model for predicting cyclic behavior of reinforcing steel." *J. Struct. Eng.* 121 (3): 433–445. https://doi.org/10.1061/(ASCE)0733-9445(1995)121:3(433).

Ebrahimian, H., R. Astroza, and J. P. Conte. 2015. "Extended Kalman filter for material parameter estimation in nonlinear structural finite element models using direct differentiation method." *Earthquake Eng. Struct. Dyn.* 44 (10): 1495–1522. https://doi.org/10.1002/eqe.2532.

Ebrahimian, H., R. Astroza, J. P. Conte, and R. A. de Callafon. 2017. "Nonlinear finite element model updating for damage identification of civil structures using batch Bayesian estimation." *Mech. Syst. Signal Process.* 84 (Feb): 194–222. https://doi.org/10.1016/j.ymssp.2016.02.002.

FEMA. 2000. *Recommended post-earthquake evaluation and repair criteria for welded steel moment-frame buildings*. FEMA 352. Washington, DC: FEMA.

FEMA. 2018. *Guidelines for performance-based seismic design of buildings*. FEMA P-58. Washington, DC: FEMA.

FEMA. 2020. *Prestandard and commentary for the seismic rehabilitation of buildings*. FEMA 356. Washington, DC: FEMA.

Foroughnia, F., V. Macchiarulo, L. Berg, M. DeJong, P. Milillo, K. W. Hudnut, K. Gavin, and G. Giardina. 2024. "Quantitative assessment of earthquake-induced building damage at regional scale using LiDAR data." *Int. J. Disaster Risk Reduct.* 106 (May): 104403. https://doi.org/10.1016/j.ijdrr.2024.104403.

Friswell, M. I., J. E. Mottershead, and H. Ahmadian. 2001. "Finite–element model updating using experimental test data: Parametrization and regularization." *Philos. Trans. R. Soc. London, Ser. A* 359 (1778): 169–186. https://doi.org/10.1098/rsta.2000.0719.

Gomes, A., and J. Appleton. 1997. "Nonlinear cyclic stress-strain relationship of reinforcing bars including buckling." *Eng. Struct.* 19 (10): 822–826. https://doi.org/10.1016/S0141-0296(97)00166-1.

Goulet, J. A., C. Michel, and A. Der Kiureghian. 2015. "Data-driven post-earthquake rapid structural safety assessment." *Earthquake Eng. Struct. Dyn.* 44 (4): 549–562. https://doi.org/10.1002/eqe.2541.

Haselton, C. B. 2006. "Assessing seismic collapse safety of modern reinforced concrete moment frame buildings." Ph.D. dissertation, Dept. of Civil and Environmental Engineering, Stanford Univ.

Hemez, F. M., and S. W. Doebling. 2001. "Review and assessment of model updating for non-linear, transient dynamics." *Mech. Syst. Signal Process.* 15 (1): 45–74. https://doi.org/10.1006/mssp.2000.1351.

Intertechnology. 2024. "Celesco extension position transducers." Accessed October 12, 2024. https://www.celesco-transducers.com/celesco-cable-position-transducers.htm.

Jaishi, B., and W.-X. Ren. 2005. "Structural finite element model updating using ambient vibration test results." *J. Struct. Eng.* 131 (4): 617–628. https://doi.org/10.1061/(ASCE)0733-9445(2005)131:4(617).

JCSS (Joint Committee for Structural Safety). 2001. *JCSS probabilistic model code*. Zurich, Switzerland: JCSS.

Liu, Y., and M. D. Shields. 2017. "A direct simulation method and lower-bound estimation for a class of gamma random fields with applications in modelling material properties." *Probab. Eng. Mech.* 47 (Jan): 16–25. https://doi.org/10.1016/j.probengmech.2017.01.001.

Mackie, K., and B. Stojadinovic. 2004. "Residual displacement and post-earthquake capacity of highway bridges." In *Proc., 13th World Conf. on Earthquake Engineering*, 1–16. Vancouver, Canada: International Association for Earthquake Engineering.

Maeda, M., Y. Nakano, and K. S. Lee. 2004. "Post-earthquake damage evaluation for R/C buildings based on residual seismic capacity." In Vol. 1179 of *Proc., 13th World Conf. on Earthquake Engineering*. Vancouver, Canada: International Association for Earthquake Engineering.

Marwala, T. 2010. *Finite element model updating using computational intelligence techniques: Applications to structural dynamics*. London: Springer.

McCormick, J., H. Aburano, M. Ikenaga, and M. Nakashima. 2008. "Permissible residual deformation levels for building structures considering both safety and human elements." In *Proc., 14th World Conf. on Earthquake Engineering*, 12–17. Beijing: Seismological Press.

Melchers, R. E., and A. T. Beck. 2018. *Structural reliability analysis and prediction*. Hoboken, NJ: Wiley.

Naeim, F., S. Hagie, A. Alimoradi, and E. Miranda. 2005. *Automated post-earthquake damage assessment and safety evaluation of instrumented buildings*. JAMA Rep. No. 2005-10639. Los Angeles: John A. Martin and Associate.

Newmark, N. M. 1959. "A method of computation for structural dynamics." *J. Eng. Mech. Div.* 85 (3): 67–94. https://doi.org/10.1061/JMCEA3.0000098.

Pampanin, S., C. Christopoulos, and M. J. Nigel Priestley. 2003. "Performance-based seismic response of frame structures including residual deformations. Part II: Multi-degree of freedom systems." *J. Earthquake Eng.* 7 (1): 119–147. https://doi.org/10.1142/S1363246903000900.

Pearl, J. 2009. *Causality.* Cambridge, UK: Cambridge University Press.

Powell, G. H., and P. F.-S. Chen. 1986. "3D beam-column element with generalized plastic hinges." *J. Eng. Mech.* 112 (7): 627–641. https://doi.org/10.1061/(ASCE)0733-9399(1986)112:7(627).

Priestley, M. J. N. 1996. *Seismic design and retrofit of bridges*. Hoboken, NJ: Wiley.

Raghunandan, M., A. B. Liel, and N. Luco. 2015. "Aftershock collapse vulnerability assessment of reinforced concrete frame structures." *Earthquake Eng. Struct. Dyn.* 44 (3): 419–439. https://doi.org/10.1002/eqe.2478.

Rathje, E. M., et al. 2017. "DesignSafe: New cyberinfrastructure for natural hazards engineering." *Nat. Hazard. Rev.* 18 (3): 06017001. https://doi.org/10.1061/(ASCE)NH.1527-6996.0000246.

Ren, W.-X., and H.-B. Chen. 2010. "Finite element model updating in structural dynamics by using the response surface method." *Eng. Struct.* 32 (8): 2455–2465. https://doi.org/10.1016/j.engstruct.2010.04.019.

Reuland, Y., P. Lestuzzi, and I. F. C. Smith. 2019. "A model-based data-interpretation framework for post-earthquake building assessment with scarce measurement data." *Soil Dyn. Earthquake Eng.* 116 (Jan): 253–263. https://doi.org/10.1016/j.soildyn.2018.10.008.

Ruiz-García, J., and E. Miranda. 2006. "Residual displacement ratios for assessment of existing structures." *Earthquake Eng. Struct. Dyn.* 35 (3): 315–336. https://doi.org/10.1002/eqe.523.

Schoettler, M. J., J. I. Restrepo, G. Guerrini, D. E. Duck, and F. Carrea. 2012. *A full-scale, single-column bridge bent tested by shake-table excitation*. PEER Rep. No. 2015/02. Reno, NV: Dept. of Civil Engineering, Center for Civil Engineering Earthquake Research, Univ. of Nevada.

Scott, M. H., and G. L. Fenves. 2006. "Plastic hinge integration methods for force-based beam–column elements." *J. Struct. Eng.* 132 (2): 244–252. https://doi.org/10.1061/(ASCE)0733-9445(2006)132:2(244).

Segura, C. L., Jr., S. Sattar, and M. A. Hariri-Ardebili. 2022. "Quantifying material uncertainty in seismic evaluations of reinforced concrete bridge column structures." *ACI Struct. J.* 119 (3): 141–152. https://doi.org/10.14359/51734486.

Su, J., Z. Li, J. Wang, and R. P. Dhakal. 2020. "Numerical simulation and damage analysis of RC bridge piers reinforced with varying yield strength steel reinforcement." *Soil Dyn. Earthquake Eng.* 130 (Mar): 106007. https://doi.org/10.1016/j.soildyn.2019.106007.

Taucer, F., E. Spacone, and F. C. Filippou. 1991. Vol. 91 of *A fiber beam-column element for seismic response analysis of reinforced concrete structures*. Berkeley, CA: Earthquake Engineering Research Center, College of Engineering, Univ. of California.

Wu, J. R., and Q. S. Li. 2004. "Finite element model updating for a high-rise structure based on ambient vibration measurements." *Eng. Struct.* 26 (7): 979–990. https://doi.org/10.1016/j.engstruct.2004.03.002.

Xiang, N., X. Chen, and M. Sharia Alam. 2020. "Probabilistic seismic fragility and loss analysis of concrete bridge piers with superelastic shape memory alloy-steel coupled reinforcing bars." *Eng. Struct.* 207 (Mar): 110229. https://doi.org/10.1016/j.engstruct.2020.110229.

Yassin, M. H. M. 1994. "Nonlinear analysis of prestressed concrete structures under monotonic and cyclic loads." Ph.D. dissertation, Dept. of Civil and Environmental Engineering, Univ. of California, Berkeley.

Yazgan, U. 2009. "The use of post-earthquake residual displacements as a performance indicator in seismic assessment." Ph.D. dissertation, Institute of Structural Engineering, Swiss Federal Institute of Technology Zurich Univ.

Yazgan, U., and A. Dazio. 2012. "Post-earthquake damage assessment using residual displacements." *Earthquake Eng. Struct. Dyn.* 41 (8): 1257–1276. https://doi.org/10.1002/eqe.1184.

Yu, R., P. Li, J. Shan, and H. Zhu. 2022a. "Structural state estimation of earthquake-damaged building structures by using UAV photogrammetry and point cloud segmentation." *Measurement* 202 (Oct): 111858. https://doi.org/10.1016/j.measurement.2022.111858.

Yu, X., X. Li, and Y. Bai. 2022b. "Evaluating maximum inter-story drift ratios of building structures using time-varying models and Bayesian filters." *Soil Dyn. Earthquake Eng.* 162 (Nov): 107496. https://doi.org/10.1016/j.soildyn.2022.107496.

Zhang, Y., H. V. Burton, H. Sun, and M. Shokrabadi. 2018. "A machine learning framework for assessing post-earthquake structural safety." *Struct. Saf.* 72 (May): 1–16. https://doi.org/10.1016/j.strusafe.2017.12.001.

Zhang, Z., and C. Sun. 2021. "Structural damage identification via physics-guided machine learning: A methodology integrating pattern recognition with finite element model updating." *Struct. Health Monit.* 20 (4): 1675–1688. https://doi.org/10.1177/1475921720927488.

Zhao, J., and S. Sritharan. 2007. "Modeling of strain penetration effects in fiber-based analysis of reinforced concrete structures." *ACI Struct. J.* 104 (2): 133–141. https://doi.org/10.14359/18525.

Zhu, M., F. McKenna, and M. H. Scott. 2018. "OpenSeesPy: Python library for the OpenSees finite element framework." *SoftwareX* 7 (Jan): 6–11. https://doi.org/10.1016/j.softx.2017.10.009.